Article:
Yao, D, Yang, H, Hu, Q et al. (3 more authors) (2021) Carbon nanotubes from post-consumer waste plastics: Investigations into catalyst metal and support material characteristics. Applied Catalysis B: Environmental, 280. 119413. ISSN 0926-3373

https://doi.org/10.1016/j.apcatb.2020.119413

Carbon nanotubes from post-consumer waste plastics: Investigations into catalyst metal and support material characteristics

Dingding Yao [ab], Haiping Yang [a], Qiang Hu [a,*], Yingquan Chen[a], Hanping Chen [a], Paul T. Williams [b,*]

[a]*State Key Laboratory of Coal Combustion, School of Energy and Power Engineering, Huazhong University of Science and Technology, 430074 Wuhan, China*

[b]*School of Chemical and Process Engineering, University of Leeds, Leeds, LS2 9JT, UK*

Abstract

Carbon nanotubes were produced from post-consumer mixed waste plastics using a pyrolysis-catalysis process. The catalysts used were Ni-Fe bimetals supported over four different porous materials. The Ni-Fe/MCM41 catalyst displayed the highest catalytic activity for the pyrolysis-catalysis of the waste plastics in terms of carbon material yield at 55.60 wt.%. The order of catalytic activity was Ni-Fe/MCM41> Ni-Fe/ZSM5> Ni-Fe/Beta> Ni-Fe/NKF5, which was closely related to their differences in catalyst pore volume and catalyst reducibility. Formation of Ni-Fe alloy with fine particle dispersion over the Ni-Fe/MCM41 catalyst is suggested to be crucial for the promotion of the decomposition of the carbon precursors and subsequent precipitation to form carbon nanotubes. Whereas, the large catalyst particle size for the Ni-Fe/Beta catalyst led to irregular carbon shapes with a simultaneous decrease in purity and graphitization of the nanotubes. By-product production of hydrogen in large quantities (38.10 mmol H_2 $g^{-1}_{plastic}$) could be used as process fuel.

Keywords: Carbon nanotubes; Plastics; Pyrolysis; Catalysis; Waste

*Corresponding authors.

E-mail address: hust_hq@163.com (Qiang Hu), p.t.williams@leeds.ac.uk (P. T. Williams);

1. Introduction

There is increasing worldwide concern in relation to the impact of the large tonnages of waste plastic on the environment [1, 2]. In response, there has been a marked rise in the collection and recycling of waste plastics, for example in Europe in 2018, 29.1 million tonnes of waste plastics were collected with 32.5% recycled, 42.6% used for energy recovery (mainly incineration) and 24.9% landfilled [3]. However, the processes used to recycle the waste plastics are almost exclusively via mechanical recycling to produce low grade plastic products [4]. The production of high value products from recycled waste plastics would significantly incentivise a rise in collection and recycling rates. One high value product that has received attention is the production of carbon nanotubes from waste plastics [5]. Carbon nanotubes have unique properties with a rapidly growing number of applications in a wide variety of industries [6]. The commercial production of carbon nanotubes is mainly through chemical vapour deposition. The process involves precursor carbon rich gases such as methane, ethylene, acetylene, benzene, etc., which interact with catalysts at high temperature (600 - 1200 °C) resulting in carbon deposition and carbon nanotube or carbon nanofiber growth on the catalyst surface [7-9]. Processes used for the production of carbon nanotubes from waste plastics usually involves a first stage of pyrolysis where the plastics are thermally degraded to produce a wide range of hydrocarbon volatiles which act as the carbon-rich precursor feedstock [10]. The hydrocarbons then pass to a second catalytic stage, for the carbon vapour deposition at high temperature (typically ~800 °C) [11-15]. It has been reported that the quality and yield of carbon nanomaterials produced from waste plastics are influenced by a range of operational conditions including temperature, steam, feedstock, feed rate, reactor type, and catalyst [13-18]. The active catalyst metals investigated have included transition metals especially Fe, Ni, Co based catalysts[14, 16, 19]. Ni is one of the most

commonly used active metals for plastic waste conversion, due to its high ability to break C-C and C-H bonds. But Fe is more cost-effective than Ni and Co. In addition, bimetallic catalysts including Ni-Fe, Ni-Cu and Fe-Mo based catalysts have been shown to possess higher activity towards carbon nanotube production [15, 20, 21]. For example, Ratkovic et al. [22] found that the yield of carbon nanotubes from the catalytic carbon vapour deposition of ethylene over Fe-Ni/Al_2O_3 catalyst was three times higher than that over a monometallic Fe based catalyst. The modification in activity and selectivity of the bimetallic catalyst was attributed to the enhanced metal-support interaction through the introduction of the second metal to the catalyst [23]. In addition, it has been shown that the agglomeration of nano-sized active metal particles can be minimised for bimetallic catalysts used for carbon nanotube production. Kutteri et al. [24] reported that bimetallic catalysts (Ni, Fe, Co supported on SiO_2) resulted in decreased crystallite size and a more stabilized catalyst for carbon nanotube production from methane. Fe-Ni bimetallic catalyst was reported to need lower activation energy for CNT growth compared with monometallic Fe and Ni catalysts [25]. The influence of different metal ratios on product distributions have been previously studied [21]. It was found that Ni-Fe catalysts with a high Fe:Ni ratio possessed high cracking ability and contributed to an increased yield of carbon nanotubes from the two-stage pyrolysis-catalysis of waste plastics.

The catalyst support material also plays a key role in the properties of the catalyst used in the chemical vapour deposition process for carbon nanotube production from waste plastics. Through metal-support interaction, the catalyst support will activate and modify the metal electronic or chemical properties, which in turn effect the hydrocarbons adsorption and dissociation [26]. In addition, we have shown for Ni-Fe bimetallic catalysts that porous γ-Al_2O_3 support material was more active compared with α-Al_2O_3 support material in the process of pyrolysis-catalysis of waste plastics for carbon nanotube production [27]. This was

attributed to the high specific surface area of the γ-Al_2O_3 support which benefitted the fine dispersion of the active Ni-Fe metals. More porous and structured silica-alumina materials for example, zeolite and MCM41 are gaining more attention as a catalyst support material compared with the more commonly used Al_2O_3 or SiO_2 supports. Li et al. [28] investigated the effect of different support materials (HZSM-5, H-Beta, and Al_2O_3) on the performance of Fe-based catalysts for the catalytic decomposition of CH_4. Compared with alumina, zeolite supported catalyst showed a lower deactivation rate, and the morphologies of the grown carbon materials were more uniform, with diameters in the range of 10-25 nm. Ahmad et al. [29] synthesized multi-walled carbon nanotubes by catalytic decomposition of acetylene on MCM-41 with Ni, Co or Fe as the active metal. The optimal condition was obtained where a high yield of carbon nanotubes was produced on a Ni/MCM-41 catalyst at 600 °C. In addition, it has been reported that these silica-alumina support materials produce aromatic hydrocarbons from the volatiles produced from plastic pyrolysis on the catalyst, leading to increased carbon deposition reactions [30, 31]. Moreover, the introduction of transition metal cations into the zeolite structure can further improve the catalyst activity towards hydrocarbon conversion.

The literature suggests that interaction of metals and bi-metal catalysts with different support materials is an interesting development for the enhanced production of carbon nanotubes from waste plastics. In this work, four types of silica-alumina materials, ZSM5, MCM41, NKF5 and H-Beta, were used as the support material to synthesise Ni-Fe based catalysts for the pyrolysis-catalysis of post-consumer waste plastics. The product carbon nanomaterials were characterised by a range of techniques to determine the influence of metal-support interaction on the yield and quality of the product carbon nanomaterials.

2. Materials and methods

2.1 Materials

The post-consumer waste plastic samples were obtained from disposed food packaging plastics, including drink cups, bottles, lunch boxes and plastic wrapping obtained from Mingjin Plastic Ltd, China. The composition of the plastic waste was ~40 wt.% high density polyethylene, ~35 wt.% low density polyethylene, ~20 wt.% polypropylene and ~5 wt.% polystyrene. The plastic waste was mixed and crushed using a liquid nitrogen grinder to yield plastic particles of size range 0.1 - 1 mm. Elemental analysis of the plastic sample showed 84.51 wt.% of carbon, 13.85 wt.% of hydrogen, 1.51 wt.% of oxygen and 0.13 wt.% of sulphur contents. The oxygen and sulphur based impurities in the plastic were derived from manufacturing additives or the waste recycling process. Proximate analysis by ASTM standards E830 and E897 showed that the ash and volatile contents of the waste plastic sample were 0.80 and 98.41 wt.% respectively. A group of porous materials obtained from Nankai University Catalyst Co. China were used as catalyst support. The supports were ZSM-5, MCM-41, NKF-5 and H-Beta, with SiO_2 to Al_2O_3 molar ratios of 38, 25, 25 and 38 respectively, and Na_2O contents of less than 0.2 wt.%. All the other chemicals including nickel and iron nitrates and ethanol regents were obtained from Sinopharm Chemical Reagent Co. China for synthesis of catalyst materials.

2.2 Catalyst preparation

The support materials were firstly calcined at 550 °C for 6 h to remove the template. The Ni-Fe based zeolite catalysts were prepared by a wet-impregnation method. A Ni to Fe molar ratio of 1:3 was chosen based on previous studies [21, 27], where results indicated that a Ni-Fe bimetallic catalyst with Ni/Fe ratio of 1:3 showed a higher activity for both quantitative

and qualitative production of carbon nanotubes than those with other Ni/Fe ratios or monometallic catalyst. In addition, since Fe had higher carbon solubility than Ni, the high Fe to Ni ratio in the Ni-Fe catalyst will be beneficial for a large amount of carbon precipitation, which is an important step for increased formation of multi-walled carbon nanotubes [32]. $Ni(NO_3)_2{\cdot}6H_2O$ and $Fe(NO_3)_3{\cdot}9H_2O$ were firstly dissolved into ethanol with continuous stirring at 50 °C, followed by addition of the support material such that a metal loading of 10 wt.% was obtained. The mixture was stirred for 4h and dried at 100 °C overnight. Afterwards, the catalyst precursors were calcined at 800 °C for 3 h of hold time in air with a heating rate of 10 °C min^{-1}. No reduction of the catalysts was carried out since the nickel and iron oxides are reduced in situ by the produced reducing gases such as H_2 during the experimentation.

2.3. Pyrolysis-catalytic reactor system

The pyrolysis-catalysis of waste plastics with the different Ni-Fe catalysts was conducted using a two stage fixed bed reactor system, as reported in our previous work [27]. This reaction system consisted of a gas supply system, a quartz tube reactor with two separately heated and temperature-controlled stages with pyrolysis of the waste plastic in the first stage followed by catalysis in the second stage. The produced pyrolysis volatiles from the waste plastic decomposition passed directly to the catalyst bed for catalytic reaction. For each experiment, 1g of plastic waste sample was placed in a quartz crucible in the middle of the pyrolysis stage. The catalyst (0.5 g) was loaded into a porous quartz crucible closely fitted within the middle of the catalysis stage where the catalysis temperature was set at 800 °C. High purity nitrogen was supplied as carrier gas at a flow rate of 100 ml min^{-1}. When the catalyst temperature reached the desired temperature, the plastic sample was heated to 500 °C at 30 °C min^{-1}, and held at the final pyrolysis temperature for 15 min. Condensable liquids

were trapped in a condensing system cooled with an ice/water mixture and non-condensable gases collected in a Tedlar gas sample bag. The product gases were analysed with an Agilent Technology (USA), Micro GC 3000 gas chromatograph (GC). The GC was a dual channel system equipped with Channel A analysing H_2, CO and CH_4 using a molecular sieve 5A column with thermal conductivity detection (TCD) and channel B analysing CO_2, C_2H_2, C_2H_4, C_2H_6 with a polystyrene column and TCD. The reproducibility of the experimental system was examined and experiments were repeated to ensure reliability.

2.4 Catalyst and carbon material characterization

The morphologies of the fresh and used catalysts were examined using a Hitachi SU8230 scanning electron microscope (SEM). Surface area and porosities of the freshly prepared catalysts was determined using a Nova-2020 instrument via N_2 adsorption/desorption isotherms at 77K. Samples were degassed at 300 °C for 2 h before analysis. The specific surface area and pore size distribution were calculated by BET and BJH methods respectively. The crystalline properties of the catalysts were determined by X-ray diffraction (XRD) with a Bruker D8 powder X-ray diffractometer operated at 40 kV and 40 mA. The temperature programmed reduction (TPR) characteristics of the fresh catalyst was characterized using a Stanton Redcroft TGH1000 thermogravimetric analyser. For each TPR determination, approximately 25 mg of fresh catalyst was heated from 25 °C to 800 °C with a heating rate of 10 °C min^{-1} in a reduction atmosphere of 5 vol.% H_2 and 95 vol.% N_2.

The yield of carbon deposition was calculated as the mass difference between freshand spent catalyst in relation to the mass of plastic feedstock [27]. The qualitative analysis of the carbon materials deposited onto the different catalysts were determined via temperature programmed oxidation (TPO) on a Shimadzu TGA-50 thermogravimetric analyser. In a

typical test, around 5 mg of the used catalyst was heated from room temperature to 800 °C at 15 °C min^{-1} in an air atmosphere and held at the final temperature for 10 min. The structure of the deposited carbon materials was observed by a high-resolution transmission electron microscope (HRTEM, FEI Tecnai TF20). Coupled with the transmission electron microscopy was elemental mapping performed with energy-dispersive X-ray spectroscopy (EDXS) using a high angle annular dark field (HAADF) imaging method. For sample preparation, the separated carbon material was dispersed in methanol in an ultrasonic bath. A sample of the solution was placed on a carbon film coated copper grid, dried and analysed using the HRTEM-EDXS system. In addition, the graphitic nature of the produced carbon material was identified using Raman spectrometry with a LabRAM HR800 Raman spectrometer (Horiba Jobin Yvon, Japan), with spectrograms obtained at a wavelength of 532 nm and with Raman shift from 200 to 3500 cm^{-1}.

3. Results and discussion

3.1 Characterization of the freshly prepared catalysts.

The morphologies of the freshly prepared catalysts were determined by SEM analysis, as shown in Fig. 1. Different shapes of crystals and particle sizes in the range of tens of nanometres to several hundred nanometres could be observed. The Ni-Fe/ZSM5 catalyst showed some rod-like particles with a diameter size of 100-300 nm in the structure. The Ni-Fe/MCM41 catalyst showed many granular crystals with very fine size (100 nm) and uniform distribution. In addition, the MCM41 supported Ni-Fe catalysts displayed the loosest structure among the four catalysts. The morphologies of NKF5 and Beta supported Ni-Fe catalysts were observed in the shape of cubic and spherical particles. Fig.1(d) showed a

number of bulk Ni-Fe/Beta catalyst particles, with size from 100 to 800 nm. Consequently, changes in the catalyst support material produced distinct differences in the physical structure of the Ni-Fe based catalysts. The BET surface area and pore volume of the freshly prepared catalysts are presented in Table 1, and the pore size distribution derived from the BJH desorption isotherms of the catalyst samples are shown in Fig. 2. The Ni-Fe/MCM41 catalyst showed the highest surface area and pore volume, at 478.80 m^2 g^{-1} and 0.539 cm^3 g^{-1} respectively. The Ni-Fe/NKF5 catalyst had almost the same surface area as the Ni-Fe/ZSM5 catalyst, but with only half of the pore volume. The difference was attributed to the relatively lower average pore size and fewer mesopores possessed by the Ni-Fe/NKF5 catalyst as demonstrated by the pore size distribution shown in Fig. 2. The Ni-Fe/MCM41 catalyst had the narrowest pore size distribution (Fig. 2) and the most intensive peak at 2.75 nm, indicating its uniform porous structure and abundant mesopores, which compared well with its higher surface area and higher pore volume compared with the other catalysts.

The crystallographic nature of the freshly prepared catalysts was studied by XRD analysis and the results are shown in Fig. 3. For most catalysts, the 2θ peaks at around 14° and 24° were derived from zeolite characteristic crystals. Pudukudy et al. [33] suggested metal oxides can be dispersed in the interior and exterior of the silica–alumina support, while the dispersion of different metals varied. The 2θ° peaks for Ni-Fe/MCM41 were extremely broad and not intense, which was due to the amorphous silica contained in MCM41. It also indicates that the Ni-Fe metals were well dispersed on the catalyst support. This corresponds with the physical structure of the catalyst shown in Fig. 1(b). The presence of Fe_2O_3 was clearly observed on both the Ni-Fe/NKF5 and Ni-Fe/Beta catalysts, with the 2θ peaks of 33.2, 35.7 and 54.4° referring to JCPDS code 01-080-5407. In addition, the peak was intensified for Ni-Fe/Beta catalyst, indicating the large crystal size and poor distribution of the active metal sites. The other diffraction peaks at 30.1, 35.8, 57.6 and 62.6° were linked to the crystal

Fe_3O_4 (JCPDS04-008-8148). It can be seen that the iron oxides were not obvious for the ZSM5 and MSM41 supported catalysts. Furthermore, the broad and weak peak from 35 to 40° on the both catalysts was hard to identify, due to the fact that several species (Fe_2O_3, Fe_3O_4, (Ni,Fe_2O_4)) all have diffractions overlapped in this range. Nickel oxide was not detected as the nickel form, with substitution of spinel structure (Ni,Fe_2O_4) found at 2θ peaks at 35.7° and 43.4° corresponding to JCPDS: 89-4927(311) and (400) plane, respectively. This suggests the insertion of Ni in the Fe lattice and the interactions between different metals during the catalyst preparation. The co-spinel structure of multi-metals were also found by others [34, 35], with demonstrated benefits of improved catalyst activity and catalyst stability. Zhang et al. [36] reported that the 2θ° peak of NiO became weaker and broader with the increase of the amount of another metal (Ru) in the catalyst with additional reduction in particle size. Therefore, the weak identification of Ni may be due to the small amount of metal loading, or the facilitated fine distribution of Ni by the introduction of Fe.

The presence of reducible metal species was determined by H_2-TPR analysis, and the results are shown in Fig. 4. A peak from the H_2 consumption thermogram represents the reducible species, while the associated temperature relates to the interaction between catalyst active sites and the support material [21]. The TPR results show that all of the prepared catalysts were completely reduced at the temperature of 800 °C. Both the MCM41 and ZSM5 supported Ni-Fe catalysts displayed two main reduction peaks, one at a temperature of around 350 °C and another at the higher reduction temperature between 500 and 700 °C. The TPR peak at low temperatures related to the bulk oxides which weakly interacted with the support material, whereas the high-temperature TPR peaks corresponded to the species which penetrate into the support to form strong interactions. According to the literature, Fe_2O_3 undergoes two reduction stages, one from Fe_2O_3 to Fe_3O_4 at around a temperature of 360°C, and another from Fe_3O_4 to Fe which occurs in the temperature range of 450~700°C [37, 38].

Bulk NiO was reported to be reduced at a temperature of 367 °C [24]. The introduction of Ni to Fe to form the Ni-Fe alloy inside the Ni-Fe/ZSM5 and Ni-Fe/MCM41 catalysts shifted the reduction temperature to low temperature areas, corresponding to a higher reducibility. The Ni-Fe/MCM41 catalyst displayed higher reducibility than the other catalysts, suggesting more active metal sites at the early reaction stage. In addition, the broad TPR peak for the Ni-Fe/MCM41 catalyst at around a temperature of 350 °C also indicates the uniform dispersion of Fe-Ni oxides with fine particle size on the surface of the catalyst [39]. In comparison to the ZSM5 and MCM supported Ni-Fe catalysts, almost no significant TPR peaks were detected below a temperature of 450 °C for the NKF5 and H-Beta based catalysts, indicating a lower reducibility. Also, a significant reduction process occurred from 550 to 800 °C assigned to the reduction of Ni-Fe oxides which had strong interaction with the support material.

3.2 Products from pyrolysis-catalysis of waste plastics

The pyrolysis of waste plastics followed by in-situ volatile catalytic reactions with four different zeolite supported catalysts was performed, and the product yields and gas composition are shown in Table 2. The total gas yield varied with a change in catalyst type with the yields between 30.8 (Ni-Fe/MCM41) to 37.8 wt.% (Ni-Fe/ZSM5). However, the solid catalyst carbon deposition varied greatly between the different catalysts due to the change in the catalyst activity of the different catalyst support materials. The Ni-Fe/MCM41 catalyst produced the highest catalyst carbon deposition at 55.60 wt.%. In addition, the Ni-Fe/MCM41 catalyst produced the lowest yield of hydrocarbon gases (CH_4 and C_{2+}) suggesting higher conversion of the plastics pyrolysis gases. Also, the maximum hydrogen yield was produced with the Ni-Fe/MCM41 catalyst at 38.1 mmol $g^{-1}_{plastic}$ and volumetric H_2 concentration of 77.46 vol.%. The high total gas yield produced from the pyrolysis-catalysis

process (30.80 - 37.8 wt.%) and high hydrogen content (between 60.26 – 77.46 vol.%) and methane content (14.41 – 27.96 vol.%) of the product gas would have sufficient energy content to enable the gas to be used as process fuel to provide the heat for the pyrolysis-catalysis reactor system.

Generally, the pyrolysis-catalysis process with the four Ni-Fe supported catalysts used in this work showed significant catalytic activity for hydrocarbon decomposition, producing higher proportions of lower molecular weight hydrocarbon gases, hydrogen and catalyst carbon deposition than the non-catalytic process as reported in our previous work [27]. The NKF5 supported Ni-Fe catalyst showed the lowest catalytic activity among the four catalysts, with the carbon deposition of 36.60 wt.% and the lowest hydrogen yield of 22.40 $mmolg^{-1}_{plastic}$ respectively. Also there was a relatively higher concentration of gaseous hydrocarbons in the product gas compared with the other catalysts with CH_4 and C_{2+} at 27.96 vol.% and 3.96 vol.% respectively.

The catalyst which generated the highest yield of catalyst carbon deposits, highest hydrogen yield and lower oil yield (Ni-Fe/MCM41) suggests that the role of the catalyst mainly acted towards catalytic thermal cracking reactions. The higher activity would contribute to increased decomposition of pyrolysis volatiles, thus producing gases and solid carbon at the expense of a decrease in the yield of pyrolysis oil. Specifically, this catalytic effect was in the form of activating and breaking of C-H bonds ($C_xH_y \rightarrow C + H_2$), resulting in more hydrogen gas and solid carbon. The differences in catalyst activity may be attributed to the different metal-support interactions as well as the catalyst selectivity for catalytic thermal cracking of pyrolysis volatiles[40]. The very strong interaction between metal and support was reported to suppress the growth of carbon nanomaterials, while too weak interaction may result in the mobility and coalescence of metal particles and further decrease the catalyst selectivity [22, 41]. Jia et al. [42] used X-Ni oxides for converting PP and PE, and concluded

that La-Ni catalyst with neither too strong or too weak interaction contributed the highest carbon yield. In the present study, NKF5 and H-Beta supported Ni-Fe catalysts had strong metal-support interaction as observed by the high reduction temperature in Fig.4, which then led to the low carbon yield. In addition, the strong metal-support was usually accompanied by low reducibility. Zhou et al. [43] reported that the catalyst activity towards hydrocarbon decomposition into carbon nanomaterials corresponded well with the catalyst reducibility. It is likely that in this work, the higher reducibility together with a moderate metal-support interaction of the Ni-Fe/MCM41 and Ni-Fe/ZSM5 catalysts produced more exposed active sites during catalytic reactions, thereby producing higher conversion of the waste plastics pyrolysis gases into gas and solid products. In addition, the catalyst performance could be linked to the porous nature of the different catalysts. Catalyst support materials with a more porous structure were always accompanied by a fine distribution of the active metals, where the reaction intermediates could have a relatively high possibility to be adsorbed and react to produce the final products [44, 45]. Therefore, it may be suggested that the porous structure of the catalyst support materials as well as the reducibility of the Ni-Fe/MCM41 catalyst contributed to the optimum conversion of the plastics pyrolysis gases to product gas and carbon deposition.

3.3 Carbon nanomaterials from pyrolysis-catalysis of waste plastics

The thermal degradation characteristics of the carbon deposits after pyrolysis-catalysis of the waste plastics in relation to the four different Ni-Fe supported catalysts were studied by TPO and the results are shown in Fig. 5. The weight loss thermograms are assigned to the oxidation of the carbon deposited on the surface of the catalyst as the oxidation temperature was increased from room temperature to 800 °C at 15 °C min^{-1} in an air atmosphere. Fig.5

shows that the catalyst mass loss was 67.92, 75.22, 45.92 and 60.59% for Ni-Fe/ZSM5, Ni-Fe/MCM41, Ni-Fe/NKF5 and Ni-Fe/Beta respectively. The highest mass loss of Ni-Fe/MCM41 was associated with the highest levels of carbon deposits, which was consistent with the data shown in Table 2. All of the carbon present on the catalysts was completely oxidised when the temperature reached 750 °C, however, different differential mass loss TPO peaks were observed for the different samples. The oxidation mass loss peak at low temperature is assigned to oxidation of amorphous carbon, while the oxidation temperature higher than 600 °C is linked to the oxidation of filamentous type carbon which possess higher thermal stability. The broad mass loss peak shown for the TPO of the Ni-Fe/ZSM5 and Ni-Fe/NKF5 catalysts may be due to an overlap of these two types of carbon. The oxidation peak in the case of Ni-Fe/MCM41 at a temperature of around 675 °C, suggests higher thermal stability of the carbon deposits linked to more filamentous carbon. Carbon deposits on the Ni-Fe/Beta catalyst showed the lowest oxidation temperature, suggesting a higher content of amorphous carbon.

SEM images of the used catalysts after pyrolysis-catalysis of the mixed plastic waste are shown in Fig. 6, which shows the presence of a dense, entangled growth of filamentous carbons covering the surface of the Ni-Fe/MCM41, Ni-Fe/ZSM5, Ni-Fe/Beta and Ni-Fe/NKF5 catalysts. The length of these carbon filaments was up to a few microns. TEM images of the catalyst carbon deposits are shown in Fig. 7, and demonstrate clearly that the produced filamentous carbon deposits were dominated by multi-walled carbon nanotubes, with some complete or incomplete bamboo-like knots identified. The Ni-Fe/ZSM5 catalyst exhibited carbon nanotubes with diameters in the range of 18 nm to 25 nm. In addition, a thin layer of amorphous carbon was observed attached on the outer walls of some carbon nanotubes at high-resolution imaging. However, almost no noticeable amorphous carbon was detected with the Ni-Fe/MCM41 catalyst (Fig. 7(a)). The thickness of the nanotube walls

with 20 carbon layers was 6.75 nm, corresponding to 0.34 nm of the lattice spacing, close to that of the graphite plane (0.335 nm) (Fig. 7(b). Also, the formed carbon nanotubes were rather uniform with diameters around 24 nm. The Ni-Fe/NKF5 catalyst produced carbon nanotubes that could be assigned to two groups, with diameters of around 22 nm and diameters of around 12 nm respectively (Fig. 7(c). The group of carbon nanotubes with smaller diameters showed an entangled structure while thicker carbon nanotubes were straighter. The diversified structure of carbon nanotubes was also found with the Ni-Fe/Beta catalyst and showed the least quality and uniformity of the produced carbons. The size of catalyst particle was suggested to be mainly responsible for the morphology, especially the diameter, of filamentous carbon. Therefore, it may be suggested that the uneven dispersion and large particles of the H-Beta support catalyst, as illustrated by XRD analysis and their physical properties (Table 1), gives rise to more complicated carbon nanotube morphologies. The carbon wrapped around large metal catalyst particles by thick carbon layers has been suggested to interrupt the growth of carbon nanotubes from metal active sites, and may be another reason for the low yield of carbon deposits [22]. Normally, there are two prevailing descriptions for the CNTs growth mechanism, tip-growth and base-growth, based on the location of particles inside the formed nanotubes [46]. However, it is difficult to conclude which growth mode was applicable for the carbon nanotubes produced in this work, as both the hollow tip and metal-included tip structures co-existed. Nevertheless, most catalyst particles were trapped either in the middle or at the end of tubes showing that tip-growth was more dominant. The formation of partial or complete bamboo-like knots as observed in Fig. 7, was reported to be linked to a tip-growth mechanism [46]. Metal-support interaction also plays an important role in the growth mechanism. It is widely accepted that strong interaction facilitates the base-growth while weak interaction brings tip-growth [24]. The TPR results in Fig. 4 showed that Ni-Fe/Beta had relatively strong metal-support interaction, that may

explain why in Fig .7 (d) (at low magnification) most bulk catalyst particles were located at the bottom of the produced carbons.

In order to further explore the growth of carbon nanotubes produced from the pyrolysis-catalysis of post-consumer waste plastics, some catalyst particles inside carbon nanotubes were examined. The characterisation techniques used were, high resolution transmission electron microscopy (HRTEM) with energy-dispersive X-ray spectroscopy (EDXS) using high angle annular dark field (HAADF) imaging, the results are shown in Fig. 8. As shown in Fig. 8(a) - 8(d), the elemental C, Ni and Fe were mapped for the carbon nanotubes produced with the Ni-Fe/MCM-41 catalyst. It can be seen that the combination of the elemental mapping of carbon, nickel and iron coincided well with the carbon nanotube morphology and the metal particles. In addition, the locations of Fe and Ni coincided, indicating that both metals resulted in the formation of an Fe-Ni alloy and actively participated in the growth of the carbon nanotubes. The elemental mapping of C, Fe, Ni for the other catalysts also showed similar results with metal particles detected inside the carbon nanotubes. For example, the HRTEM image of typical particles from the used Ni-Fe/NKF catalyst revealed an interlayer spacing of 2.07Å (Fig.8(e) and 8(f)), which could be assigned to the (111) plane of the Ni-Fe alloy. The formation of Fe-Ni alloy was reported to be an essential active phase for the growth of carbon nanotubes [47]. The deformation of the active metal particles, for example the elongated, and the drop-shaped particle in Fig.8(g) was attributed to the diffusion of metal within the carbon on the catalyst. However, in some cases as illustrated in Fig.8(f), where the catalyst particle was totally wrapped with several graphite layers, the continuous nucleation of carbon for further CNTs formation was interrupted by the occurrence of a carbon nano-onion (CNO) structure. This kind of CNO was formed, as explained by Zhou et al. [43], due to the imbalance between compressive force from adjacent carbon atoms and surface tension in the catalyst particle; in which case the precipitation of carbon atoms was extremely fast,

resulting in the particle being totally encapsulated by graphite layers. Such interrupted growth often occurs with large catalyst particles and would lead to only a few graphite layers being formed, which may also explain the low carbon yield with the Ni-Fe/NKF5 and Ni-Fe/Beta catalysts.

The used catalysts after pyrolysis-catalysis of the post-consumer plastics reaction were also analysed by X-ray diffraction to determine the presence of graphitic carbon and the crystalline Fe-Ni alloy. The results are shown in Fig.9. The sharp diffraction peak observed at 2θ at around 26° corresponded to the crystalline plane (002) of the obtained graphitized carbon. The d-spacing of such crystalline carbon can be determined using Bragg's equation ($d = \lambda/2 \sin\theta$) as 0.3418, 0.3418, 0.3393, 0.3420 nm for the Ni-Fe/ZSM5, Ni-Fe/MCM41, Ni-Fe/NKF5, and Ni-Fe/Beta catalysts respectively. It is clear that these values approach the identical d-spacing of graphite, at 0.3354 nm, indicating the high graphitic quality of the obtained carbon nanotubes. The significant diffraction peaks at 2θ values of 43.53°, 50.70° and 74.53° were assigned to (111), (200) and (220) crystalline planes of Ni-Fe alloy, which agreed well with the HRTEM results shown in Fig. 8.

In order to investigate the purity and graphitization of the product carbon materials on the used catalysts, Raman spectroscopy was conducted and the resultant spectra are shown in Fig. 10. The D peak at a wavelength of ~1330 cm^{-1} may be attributed to structural imperfection or amorphous carbon, while the G peak at 1560 cm^{-1} can be linked to the vibration of graphene sheets [48]. The I_D to I_G ratio was calculated as an index of defects and the degree of graphitization of the carbon nanomaterials. The intensity of the G' band at a wavelength of ~2700 cm^{-1}, is associated with the process of two-photon elastic scattering, and can also be used to estimate the purity of the carbon deposited on the catalysts. For the four investigated catalysts, the minimum I_D/I_G ratio of 0.51 was obtained with the Ni-Fe/MCM41 catalyst, suggesting that the carbon nanotubes had fewer defects and higher graphitic nature for this

catalyst compared with those produced with the other catalysts. The Raman spectra I_D/I_G ratio of the carbon nanomaterials obtained with the ZSM5 and NKF supported Ni-Fe catalysts indicated moderate purity and rather similar quality, which agreed well with the quality evaluation from the TPO thermograms (Fig. 5) where the carbon deposition on the catalyst showed very similar oxidization profiles. Compared with the Ni-Fe/NKF5 catalyst, the higher I_D/I_G ratio of the Ni-Fe/Beta catalyst implies poor quality of carbon nanotubes, though it produced a higher yield of carbon deposits (Table 2). This is consistent with the results from the TPO thermograms, as the lower reflection peak of the Ni-Fe/Beta catalyst compared with that of the Ni-Fe/NKF5 catalyst indicated a higher complexity and lower purity of carbon nanotubes. It is also worthy of note that in this study, there was a strong positive correlation between the pore volume, catalyst reducibility and carbon yield from the pyrolysis-catalysis of the waste plastics, and results followed the same order of Ni-Fe/MCM41> Ni-Fe/ZSM5> Ni-Fe/Beta> Ni-Fe/NKF5. However, in regard to the quality/graphitization of the obtained carbon materials, there was more of a closer association with the dispersion of the active metal catalyst particles. The Ni-Fe/Beta catalyst with poor active metal distribution (demonstrated by XRD analysis of the freshly prepared catalyst, and TEM characterisation of the used catalysts) generated carbon nanotubes with low purity and a lower degree of graphitization. The consistent findings of quality evaluation could be obtained from both TPO analysis and Raman spectral analysis.

In comparison with recent work on CNTs from plastic waste, Yang et al. [49] combined the use of Ni/Al-SBA-15 and Ni-Cu/CaO-SiO_2 catalyst in a fluidized catalytic bed system for continuous production of CNTs, where the highest CNTs fraction of 69.0% (corresponding to 22.25 g carbons in relation to 198 g PP and LDPE mixture) was achieved at 700 °C. Jia et al. [42] obtained a carbon yield of 86.4 % from 1.5 g feedstock of PP (equivalent to 0.23 g g^{-1}_{PP}) with Ni-La oxides. Aboul-Enein and Awadallah [15] investigated the effect of Fe/Mo ratio on

a MgO supported bimetallic Fe–Mo catalyst for production of carbon nanomaterials from LDPE, and the optimal yield reached 976% of catalyst mass (0.325 g g^{-1} $_{LDPE}$) at a Fe:Mo weight ratio of 30:20. In our previous study using the same reactor [27], the maximum carbon deposition yield of 40.7 wt.% with a γ-Al_2O_3 supported Ni-Fe catalyst was obtained. Fe/Al_2O_3 catalyst studied by Gou et al. [50], generated CNTs with a yield of 34.39 wt.% and the purity I_D/I_G ratio of 0.55 from hard plastic. It can be seen that the Ni-Fe/MCM-41 investigated in this work displayed a competitive and even better activity towards high-yield and high-purity production of carbon nanotubes from post-consumer waste plastics.

4. Conclusions

Four Ni-Fe catalysts with different support material, MCM41, ZSM5, H- Beta and NKF5, with different silica-alumina ratios, surface areas and porosities were synthesized and used for the pyrolysis-catalysis of post-consumer waste plastics for the production of multi-walled carbon nanotubes. The catalysts with different physicochemical properties exhibited different catalytic activity towards the production of the multi-walled carbon nanotubes. The highest yield of catalyst carbon deposition was obtained with the Ni-Fe/MCM41 catalyst which possessed the highest surface area and abundant mesoporous structure, thereby providing more opportunities for the interaction between reaction intermediates and catalyst active sites. The catalyst activity for the decomposition of plastic pyrolysis volatiles to produce the catalyst carbon material follow the order of Ni-Fe/MCM41> Ni-Fe/ZSM5> Ni-Fe/Beta> Ni-Fe/NKF5, which was related to the pore volume, metal-support interaction and reducibility of the catalysts. SEM and TEM analysis confirmed the deposited carbon products from the pyrolysis-catalysis of waste plastics were mostly multi-walled carbon nanotubes, with outer diameters from 12 to 25 nm. Compositional and crystalline analysis of the carbon nanotubes

revealed that the Ni-Fe alloy particles catalysed the growth of carbon nanotubes. The purity and the graphitization of carbon nanotubes were determined by TPO and Raman spectroscopy, and showed that the carbon nanotubes produced with the Ni-Fe/MCM41 catalyst displayed the highest quality, followed by the carbon nanotubes produced with the Ni-Fe/ZSM5 catalyst. However, the Ni-Fe/Beta catalysts, with poor active metal dispersion, led to the production of carbon nanotubes with disordered morphology and low degree of graphitisation. The present study suggests that the characteristics of catalyst metal, support material, and specifically the metal dispersion, metal-support interaction and active composition, had a great influence on the quantity and quality of the obtained carbon nanomaterials. This will be helpful for future catalyst design in the area of recovering value added carbon nanomaterials from low-cost plastic waste. Though the catalyst synthesized in this work generated high carbon yield (up to 55.6 wt.%), the modification of catalyst materials to produce more homogeneous and high-quality carbon nanotubes which meet the market specifications is still challenging and needs further research.

Acknowledgements

This work was carried out with financial support from National Key Research and Development Project of China (2018YFC1901204). The sample characterisations were assisted by the Analytical and Testing Centre at Huazhong University of Science & Technology, and the Analysis Laboratory in the School of Chemical and Process Engineering at the University of Leeds.

References

[1] J.R. Jambeck, R. Geyer, C. Wilcox, T.R. Siegler, M. Perryman, A. Andrady, R. Narayan, K.L. Law, Plastic waste inputs from land into the ocean, Science, 347 (2015) 768-771.

[2] M. Shahabuddin, B.B. Krishna, T. Bhaskar, G. Perkins, Advances in the thermo-chemical production of hydrogen from biomass and residual wastes: Summary of recent techno-economic analyses, Bioresource Technology, 299 (2020) 122557.

[3] Plastics – the Facts 2019, Plastics Europe, Brussels, (2019).

[4] Plastics – the Facts 2017, Plastics Europe, Brussels, (2017).

[5] A. Bazargan, G. McKay, A review - Synthesis of carbon nanotubes from plastic wastes, Chemical Engineering Journal, 195-196 (2012) 377-391.

[6] M.F. De Volder, S.H. Tawfick, R.H. Baughman, A.J. Hart, Carbon nanotubes: present and future commercial applications, Science, 339 (2013) 535-539.

[7] E. Joselevich, H. Dai, J. Liu, K. Hata, A. H. Windle, Carbon Nanotube Synthesis and Organization, in: A. Jorio, G. Dresselhaus, M.S. Dresselhaus (Eds.) Carbon Nanotubes: Advanced Topics in the Synthesis, Structure, Properties and Applications, Springer Berlin Heidelberg, Berlin, Heidelberg, 2008, pp. 101-165.

[8] M. Kumar, Carbon nanotube synthesis and growth mechanism, in: S. Yellampalli (Ed.) Carbon Nanotubes-Synthesis, Characterization, Applications, Intech, 2011, pp. 147-170.

[9] A. Chatterjee, B.L. Deopura, Carbon nanotubes and nanofibre: An overview, Fibers and Polymers, 3 (2002) 134-139.

[10] P.T. Williams, Hydrogen and Carbon Nanotubes from Pyrolysis-Catalysis of Waste Plastics: A Review, Waste and Biomass Valorization, (2020).

[11] Y.-w. Yen, M.-D. Huang, F.-J. Lin, Synthesize carbon nanotubes by a novel method using chemical vapor deposition-fluidized bed reactor from solid-stated polymers, Diamond and Related Materials, 17 (2008) 567-570.

[12] N. Mishra, G. Das, A. Ansaldo, A. Genovese, M. Malerba, M. Povia, D. Ricci, E. Di Fabrizio, E. Di Zitti, M. Sharon, M. Sharon, Pyrolysis of waste polypropylene for the synthesis of carbon nanotubes, Journal of Analytical and Applied Pyrolysis, 94 (2012) 91-98.

[13] J.C. Acomb, C. Wu, P.T. Williams, The use of different metal catalysts for the simultaneous production of carbon nanotubes and hydrogen from pyrolysis of plastic feedstocks, Applied Catalysis B: Environmental, 180 (2016) 497-510.

[14] R.-X. Yang, K.-H. Chuang, M.-Y. Wey, Effects of Temperature and Equivalence Ratio on Carbon Nanotubes and Hydrogen Production from Waste Plastic Gasification in Fluidized Bed, Energy & Fuels, 32 (2018) 5462-5470.

[15] A.A. Aboul-Enein, A.E. Awadallah, Production of nanostructured carbon materials using Fe–Mo/MgO catalysts via mild catalytic pyrolysis of polyethylene waste, Chemical Engineering Journal, 354 (2018) 802-816.

[16] Y. Shen, W. Gong, B. Zheng, L. Gao, Ni–Al bimetallic catalysts for preparation of multiwalled carbon nanotubes from polypropylene: Influence of the ratio of Ni/Al, Applied Catalysis B: Environmental, 181 (2016) 769-778.

[17] C. Wu, M.A. Nahil, N. Miskolczi, J. Huang, P.T. Williams, Processing Real-World Waste Plastics by Pyrolysis-Reforming for Hydrogen and High-Value Carbon Nanotubes, Environmental Science & Technology, 48 (2014) 819-826.

[18] S.S. Sharma, V.S. Batra, Production of hydrogen and carbon nanotubes via catalytic thermo-chemical conversion of plastic waste: review, Journal of Chemical Technology & Biotechnology, 95 (2020) 11-19.

[19] J.C. Acomb, C. Wu, P.T. Williams, Control of steam input to the pyrolysis-gasification of waste plastics for improved production of hydrogen or carbon nanotubes, Applied Catalysis B: Environmental, 147 (2014) 571-584.

[20] A.A. Aboul-Enein, A.E. Awadallah, Production of nanostructure carbon materials via non-oxidative thermal degradation of real polypropylene waste plastic using La2O3 supported Ni and Ni–Cu catalysts, Polymer Degradation and Stability, 167 (2019) 157-169.

[21] D. Yao, C. Wu, H. Yang, Y. Zhang, M.A. Nahil, Y. Chen, P.T. Williams, H. Chen, Co-production of hydrogen and carbon nanotubes from catalytic pyrolysis of waste plastics on Ni-Fe bimetallic catalyst, Energy Conversion and Management, 148 (2017) 692-700.

[22] S. Ratkovic, D. Vujicic, E. Kiss, G. Boskovic, O. Geszti, Different degrees of weak metal–support interaction in Fe–(Ni)/Al2O3 catalyst governing activity and selectivity in carbon nanotubes' production using ethylene, Materials Chemistry Physics, 129 (2011) 398-405.

[23] J. Lu, Y. Lei, G. Wan, Z. Mei, J. Yu, Y. Zhao, S. He, Y. Luo, Weakening the metal-support strong interaction to enhance catalytic performances of alumina supported Ni-based catalysts for producing hydrogen, Applied Catalysis B: Environmental, (2019) 118177.

[24] D. Ayillath Kutteri, I.W. Wang, A. Samanta, L. Li, J. Hu, Methane decomposition to tip and base grown carbon nanotubes and COx-free H2 over mono- and bimetallic 3d transition metal catalysts, Catalysis Science & Technology, 8 (2018) 858-869.

[25] W.-H. Chiang, R.M. Sankaran, Synergistic Effects in Bimetallic Nanoparticles for Low Temperature Carbon Nanotube Growth, Advanced Materials, 20 (2008) 4857-4861.

[26] Z. Liu, D.C. Grinter, P.G. Lustemberg, T.D. Nguyen-Phan, Y. Zhou, S. Luo, I. Waluyo, E.J. Crumlin, D.J. Stacchiola, J. Zhou, Dry Reforming of Methane on a Highly-Active Ni-CeO2 Catalyst: Effects of Metal-Support Interactions on C− H Bond Breaking, Angewandte Chemie International Edition, 55 (2016) 7455-7459.

[27] D. Yao, Y. Zhang, P.T. Williams, H. Yang, H. Chen, Co-production of hydrogen and carbon nanotubes from real-world waste plastics: Influence of catalyst composition and operational parameters, Applied Catalysis B: Environmental, 221 (2018) 584-597.

[28] X. Li, G. Zhu, S. Qi, J. Huang, B. Yang, Simultaneous production of hythane and carbon nanotubes via catalytic decomposition of methane with catalysts dispersed on porous supports, Applied Energy, 130 (2014) 846-852.

[29] A. Ahmad, M.H. Razali, K. Kassim, K.A. Mat Amin, Synthesis of multiwalled carbon nanotubes supported on M/MCM-41 (M = Ni, Co and Fe) mesoporous catalyst by chemical vapour deposition method, Journal of Porous Materials, 25 (2018) 433-441.

[30] Y.-K. Park, J.S. Jung, J. Jae, S.B. Hong, A. Watanabe, Y.-M. Kim, Catalytic fast pyrolysis of wood plastic composite over microporous zeolites, Chemical Engineering Journal, 377 (2018) 119742.

[31] M.Z. Siddiqui, Y.-K. Park, Y. Kang, A. Watanabe, S. Kim, Y.-M. Kim, Effective use of aluminum-plastic laminate as a feedstock for catalytic pyrolysis over micro and mesoporous catalysts, Journal of Cleaner Production, 229 (2019) 1093-1101.

[32] W.-H. Chiang, R.M. Sankaran, The influence of bimetallic catalyst composition on single-walled carbon nanotube yield, Carbon, 50 (2012) 1044-1050.

[33] M. Pudukudy, Z. Yaakob, Z.S. Akmal, Direct decomposition of methane over SBA-15 supported Ni, Co and Fe based bimetallic catalysts, Applied Surface Science, 330 (2015) 418-430.

[34] Q. Guan, Z. Kong, Z. Xie, Y. Chen, S. Chen, S. Tian, P. Ning, Catalytic gasification of phenol in supercritical water over bimetallic Co–Ni/AC catalyst, Environmental technology, 40 (2019) 2182-2190.

[35] Y. Xie, Y. Su, P. Wang, S. Zhang, Y. Xiong, In-situ catalytic conversion of tar from biomass gasification over carbon nanofibers-supported Fe-Ni bimetallic catalysts, J Fuel Processing Technology, 182 (2018) 77-87.

[36] J. Zhang, A. Dasgupta, Z. Chen, D. Xu, P.E. Savage, Y. Guo, Supercritical water gasification of phenol over Ni-Ru bimetallic catalysts, Water research, 152 (2019) 12-20.
[37] W. Li, M. Wei, Y. Liu, Y. Ye, S. Li, W. Yuan, M. Wang, D. Wang, Catalysts evaluation for production of hydrogen gas and carbon nanotubes from the pyrolysis-catalysis of waste tyres, International Journal of Hydrogen Energy, 44 (2019) 19563-19572.
[38] M. Ding, J. Tu, M. Qiu, T. Wang, L. Ma, Y. Li, Impact of potassium promoter on Cu–Fe based mixed alcohols synthesis catalyst, Applied Energy, 138 (2015) 584-589.
[39] H.-S. Roh, H. Potdar, K.-W. Jun, J.-W. Kim, Y.-S. Oh, Carbon dioxide reforming of methane over Ni incorporated into Ce–ZrO2 catalysts, Applied Catalysis A: General, 276 (2004) 231-239.
[40] N.N. Nassar, C.A. Franco, T. Montoya, F.B. Cortés, A. Hassan, Effect of oxide support on Ni–Pd bimetallic nanocatalysts for steam gasification of n-C7 asphaltenes, Fuel, 156 (2015) 110-120.
[41] J. Wang, B. Shen, M. Lan, D. Kang, C. Wu, Carbon nanotubes (CNTs) production from catalytic pyrolysis of waste plastics: The influence of catalyst and reaction pressure, Catalysis Today, 351 (2020) 50-57.
[42] J. Jia, A. Veksha, T.-T. Lim, G. Lisak, In situ grown metallic nickel from X–Ni (X=La, Mg, Sr) oxides for converting plastics into carbon nanotubes: Influence of metal–support interaction, Journal of Cleaner Production, 258 (2020) 120633.
[43] L. Zhou, L.R. Enakonda, M. Harb, Y. Saih, A. Aguilar-Tapia, S. Ould-Chikh, J.-l. Hazemann, J. Li, N. Wei, D. Gary, Fe catalysts for methane decomposition to produce hydrogen and carbon nano materials, Applied Catalysis B: Environmental, 208 (2017) 44-59.
[44] D. Yao, H. Yang, H. Chen, P.T. Williams, Co-precipitation, impregnation and so-gel preparation of Ni catalysts for pyrolysis-catalytic steam reforming of waste plastics, Applied Catalysis B: Environmental, 239 (2018) 565-577.
[45] G. Urdiana, R. Valdez, G. Lastra, M. Valenzuela, A. Olivas, Production of hydrogen and carbon nanomaterials using transition metal catalysts through methane decomposition, Materials Letters, 217 (2018) 9-12.
[46] M. Lin, J.P.Y. Tan, C. Boothroyd, K.P. Loh, E.S. Tok, Y.-L. Foo, Dynamical observation of bamboo-like carbon nanotube growth, Nano letters, 7 (2007) 2234-2238.
[47] Y. Li, D. Li, G. Wang, Methane decomposition to COx-free hydrogen and nano-carbon material on group 8–10 base metal catalysts: a review, Catalysis Today, 162 (2011) 1-48.

[48] M. Pudukudy, Z. Yaakob, Methane decomposition over Ni, Co and Fe based monometallic catalysts supported on sol gel derived SiO2 microflakes, Chemical Engineering Journal, 262 (2015) 1009-1021.

[49] R.-X. Yang, S.-L. Wu, K.-H. Chuang, M.-Y. Wey, Co-production of carbon nanotubes and hydrogen from waste plastic gasification in a two-stage fluidized catalytic bed, Renewable Energy, 159 (2020) 10-22.

[50] X. Gou, D. Zhao, C. Wu, Catalytic conversion of hard plastics to valuable carbon nanotubes, Journal of Analytical and Applied Pyrolysis, 145 (2020) 104748.

FIGURE CAPTIONS

Fig. 1. SEM images of the freshly prepared catalysts, (a) Ni-Fe/ZSM5, (b) Ni-Fe/MCM41, (c) Ni-Fe/NKF5, and (d) Ni-Fe/Beta

Fig. 2. Pore size distribution of the freshly prepared catalysts.

Fig. 3. X-ray diffraction profiles of the freshly prepared Ni-Fe catalysts.

Fig.4. Temperature programmed reduction (TPR) analysis of the freshly prepared Ni-Fe catalysts.

Fig. 5. Temperature programmed oxidation and derivative thermograms of carbon deposits over reacted catalysts.

Fig. 6. SEM images of the used catalysts (a) Ni-Fe/ZSM5, (b) Ni-Fe/MCM41, (c) Ni-Fe/NKF5, and (d) Ni-Fe/Beta

Fig. 7. TEM imaging of carbon nanomaterials at different magnifications over (a) Ni-Fe/ZSM5, (b) Ni-Fe/MCM41, (c) Ni-Fe/NKF5, and (d) Ni-Fe/Beta

Fig. 8 HRTEM and HRTEM-EDXS with HAADF analysis of the carbon deposits from the used catalysts, (a-d) HAADF-TEM and C, Ni and Fe element mapping produced with the Ni-Fe/MCM-41 catalyst; (e-f) HRTEM of the carbon nanotubes produced with the Ni-Fe/NKF5 catalyst; (g) HRTEM of carbon nanotubes with the Ni-Fe/Beta catalyst and (h) EDXS analysis of marked area 2 in (e) (Ni-Fe/Beta catalyst).

Fig. 9. XRD analysis of the used catalysts

Fig. 10. Raman spectra of the carbon over different catalysts

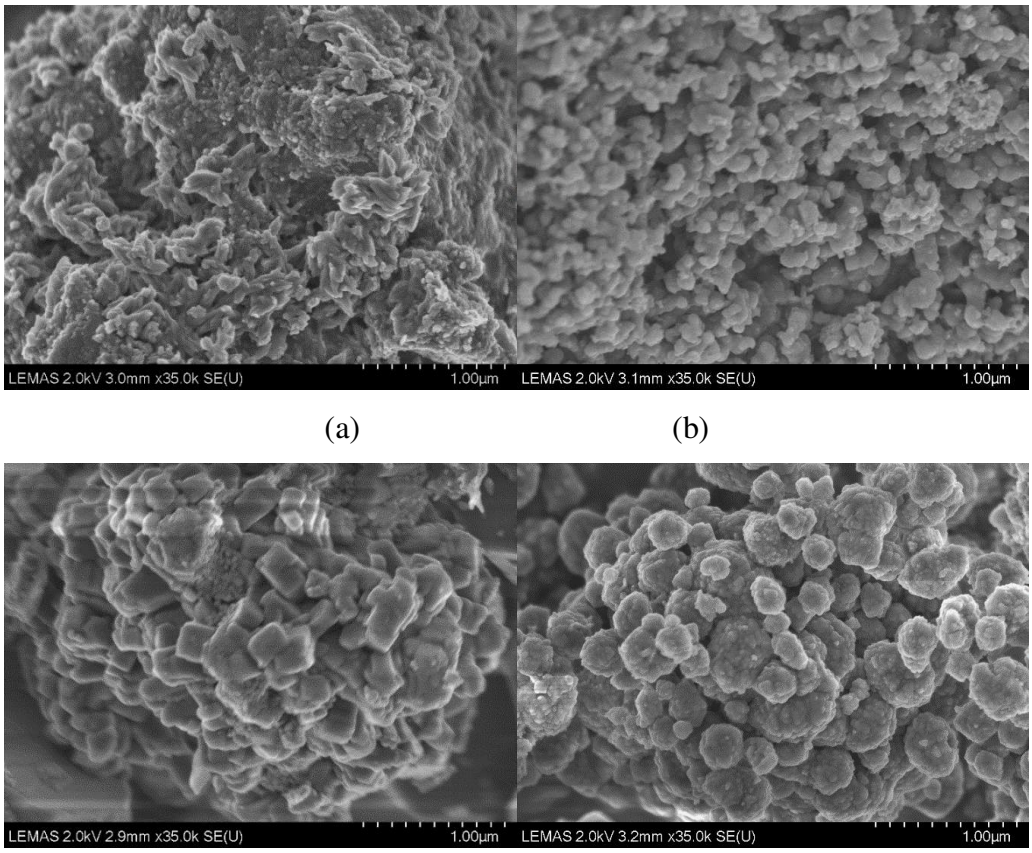

Fig. 1. SEM images of the freshly prepared catalysts, (a) Ni-Fe/ZSM5, (b) Ni-Fe/MCM41, (c) Ni-Fe/NKF5, and (d) Ni-Fe/Beta

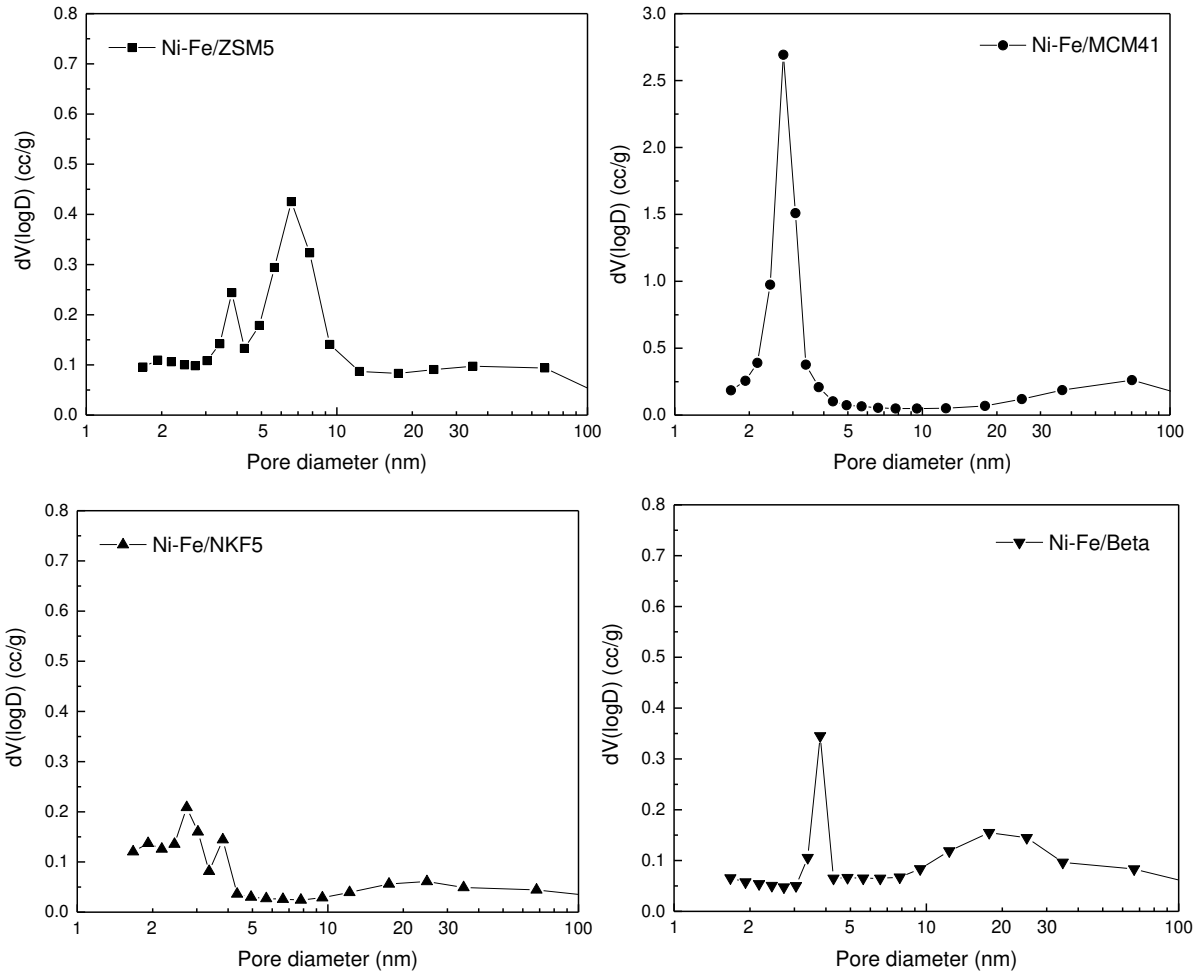

Fig. 2. Pore size distribution of the freshly prepared catalysts.

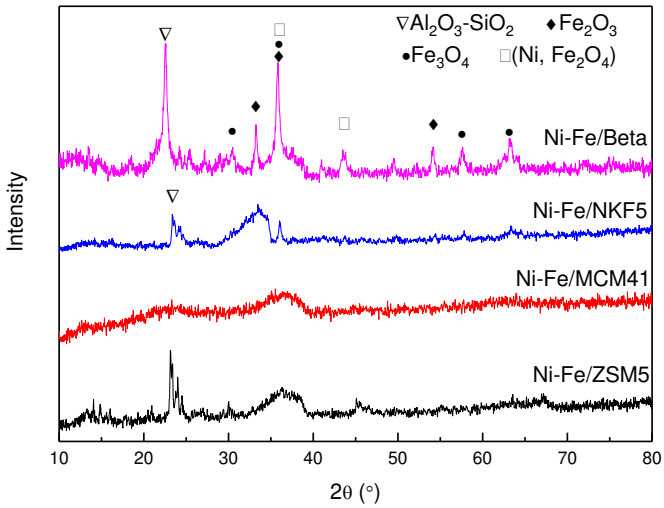

Fig. 3. X-ray diffraction profiles of the freshly prepared Ni-Fe catalysts.

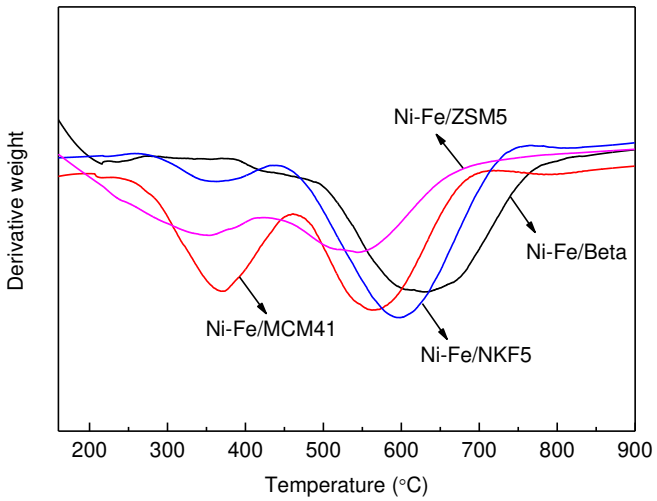

Fig.4. Temperature programmed reduction (TPR) analysis of the freshly prepared Ni-Fe catalysts.

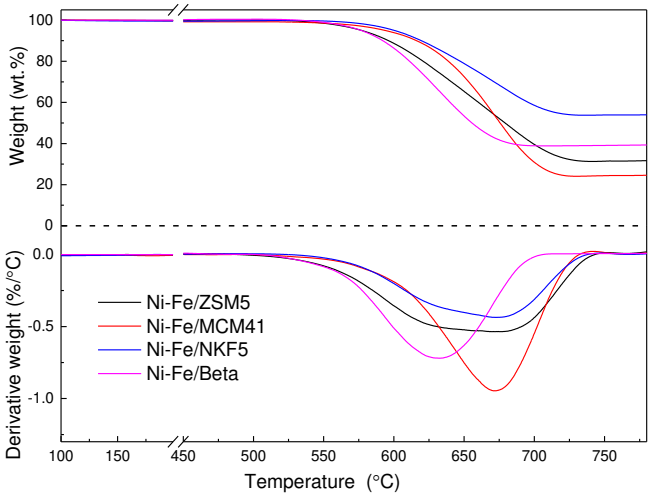

Fig. 5. Temperature programmed oxidation and derivative thermograms of carbon deposits over reacted catalysts.

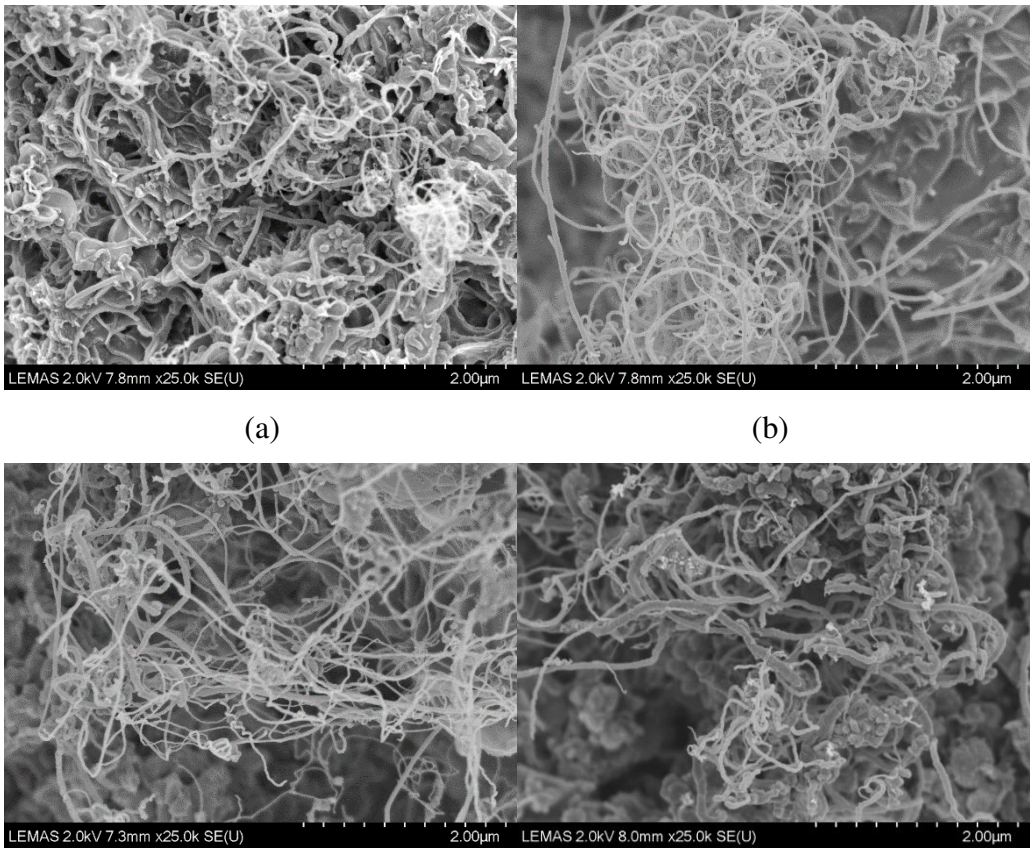

Fig. 6. SEM images of the used catalysts (a) Ni-Fe/ZSM5, (b) Ni-Fe/MCM41, (c) Ni-Fe/NKF5, and (d) Ni-Fe/Beta

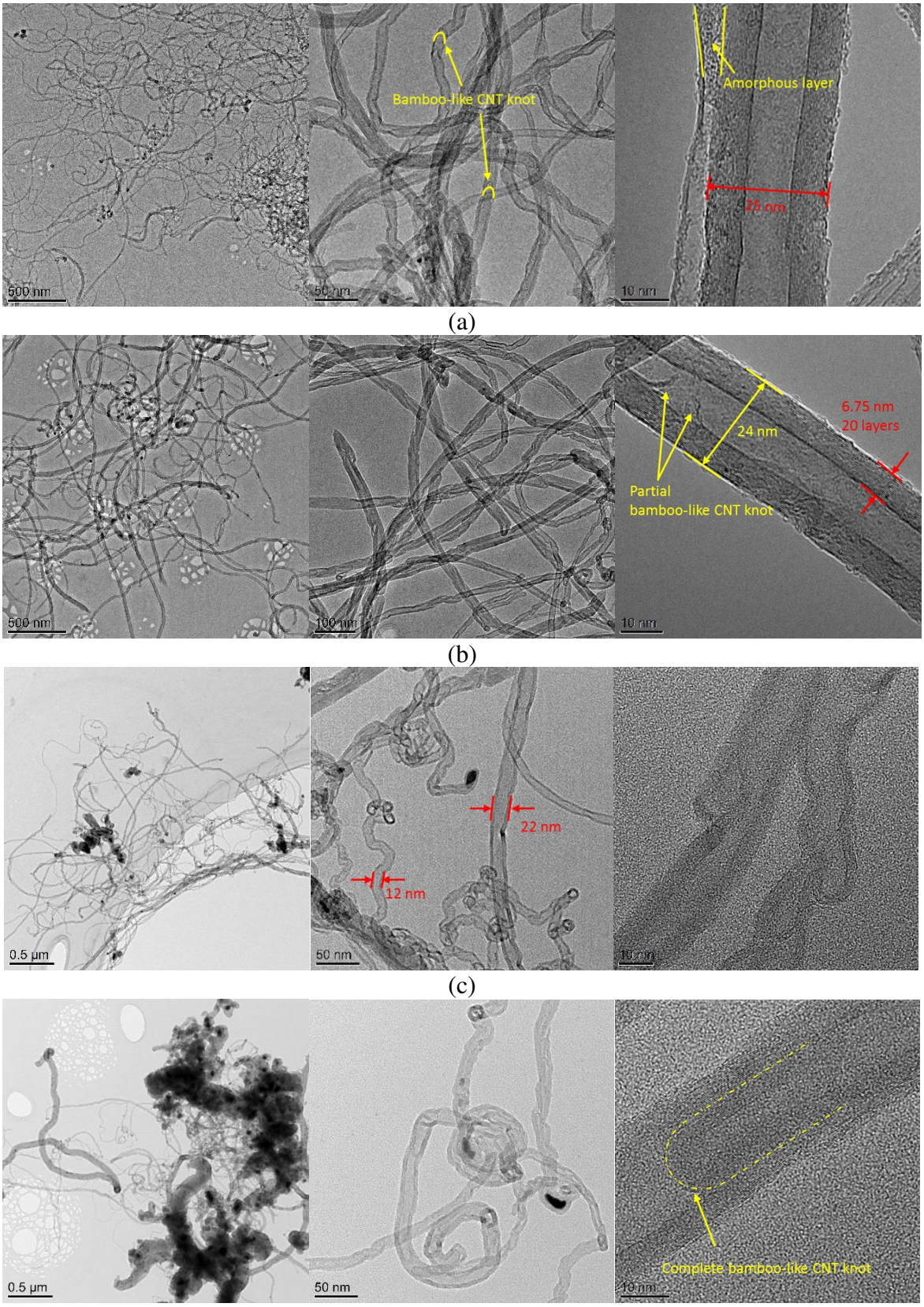

Fig. 7. TEM imaging of carbon nanomaterials at different magnifications over (a) Ni-Fe/ZSM5, (b) Ni-Fe/MCM41, (c) Ni-Fe/NKF5, and (d) Ni-Fe/Beta

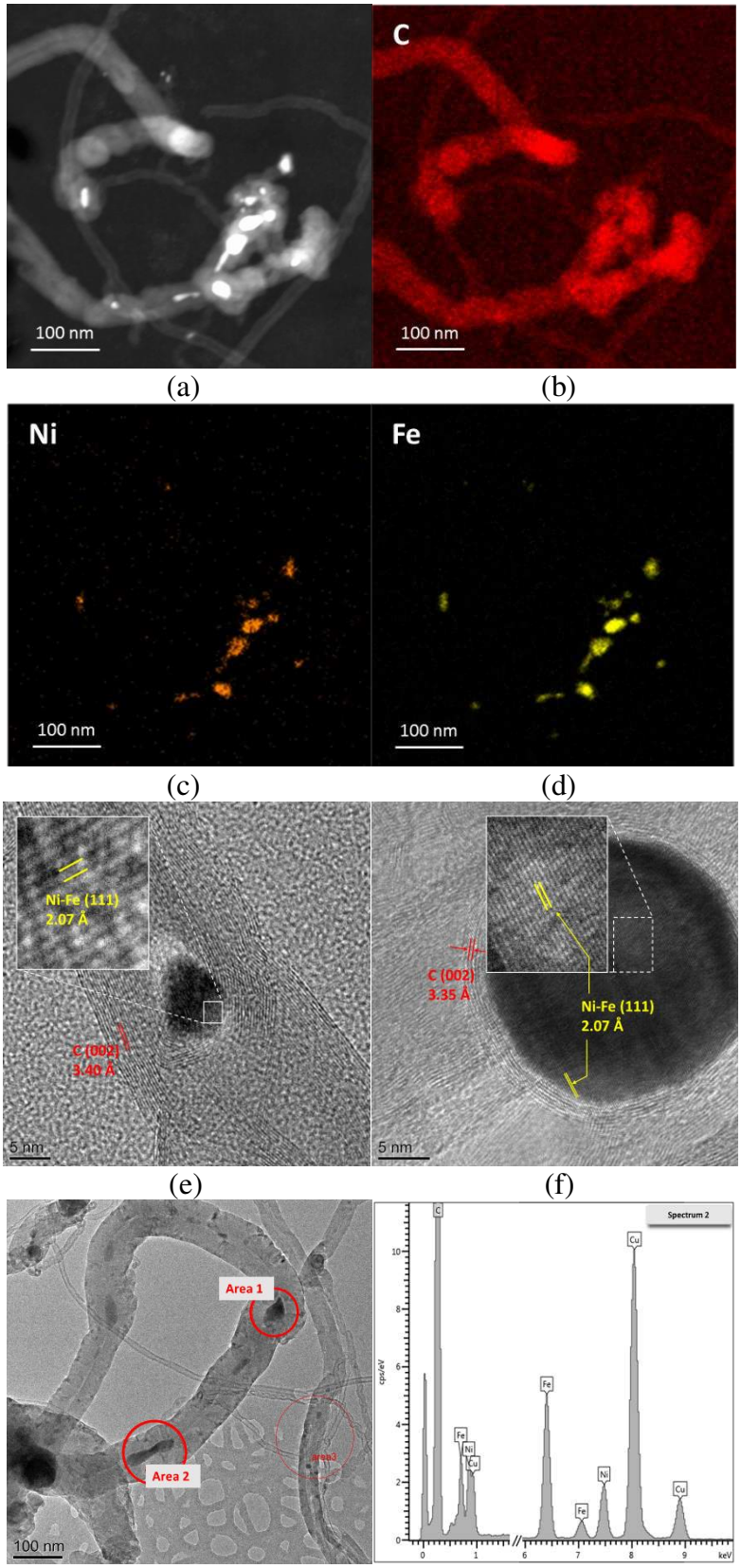

Fig. 8 HRTEM and HRTEM-EDXS with HAADF analysis of the carbon deposits from the used catalysts, (a-d) HAADF-TEM and C, Ni and Fe element mapping produced with the Ni-Fe/MCM-41 catalyst; (e-f) HRTEM of the carbon nanotubes produced with the Ni-Fe/NKF5 catalyst; (g) HRTEM of carbon nanotubes with the Ni-Fe/Beta catalyst and (h) EDXS analysis of marked area 2 in (e) (Ni-Fe/Beta catalyst).

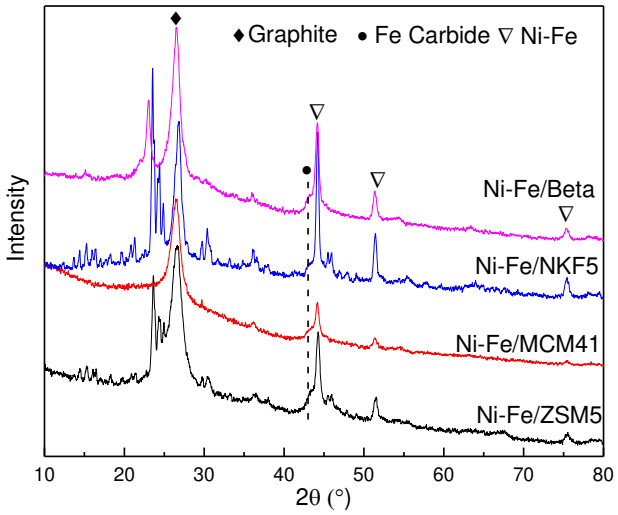

Fig. 9. XRD analysis of the used catalysts

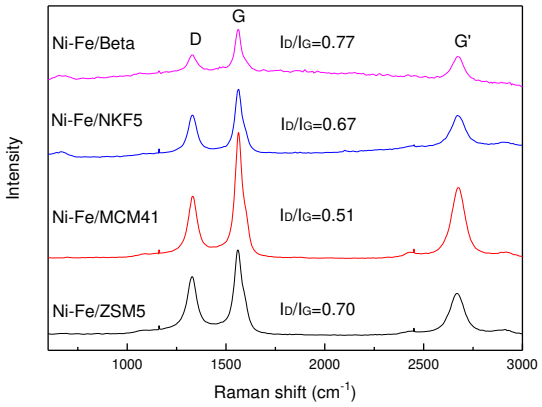

Fig. 10. Raman spectra of the carbon over different catalysts.

Table 1. Physical properties of the freshly prepared catalysts.

	BET surface area, m^2g^{-1}	**Pore volume, cm^3g^{-1}**
Ni-Fe/ZSM5	254.83	0.248
Ni-Fe/MCM41	478.80	0.539
Ni-Fe/NKF5	255.09	0.123
Ni-Fe/Beta	318.21	0.215

Table 2. Product yield and gas composition for the catalytic pyrolysis of post-consumer waste plastics using different Ni-Fe catalysts.

	Ni-Fe/ZSM5	**Ni-Fe/MCM41**	**Ni-Fe/NKF5**	**Ni-Fe/Beta**
Gas yield (wt. %)	37.80	30.80	34.00	32.10
Oil (wt. %)	17.00	16.30	27.40	15.10
Carbon deposition (wt. %)	50.00	55.60	36.60	47.00
H_2 yield (mmol H_2 $g^{-1}_{plastic}$)	35.80	38.10	22.40	32.80
Gas composition (vol.%)				
H_2	70.16	77.46	60.26	72.44
CO	0.89	0.77	1.16	0.62
CH_4	20.72	14.41	27.96	18.04
CO_2	5.74	5.74	7.56	6.78
C_{2+}	1.62	1.62	3.06	2.13